Geophys. J. Int. (2004) **159,** 435–444 doi: 10.1111/j.1365-246X.2004.02422.x

The hydroelectric problem of porous rocks: inversion of the position of the water table from self-potential data

A. Revil, V. Naudet and J. D. Meunier

CNRS-CEREGE, Université Aix-Marseille 3, *Europôle de l'Arbois,* BP 80, 13545 *Aix-en-Provence, Cedex* 4, *France*

Accepted 2004 July 19. Received 2004 July 8; in original form 2003 May 7

SUMMARY

The self-potential (SP) method is a fast and cheap reconnaissance tool sensitive to ground water flow in unconfined aquifers. A model based on the use of Green's functions for the coupled hydroelectric problem yields an integral equation relating the SP field to the distribution of the piezometric head describing the phreatic surface and to the electrical resistivity contrast through this phreatic surface. We apply this model to SP data measured on the south flank of the Piton de la Fournaise volcano, a large shield volcano located on Réunion island, Indian ocean. The phreatic surface, inverted with the help of the Simplex algorithm from the SP data, agrees well with the available information in this area [one borehole and electromagnetic (EM) data]. This interpretation scheme, which we call electrography, has many applications to the crucial problem of water supply in volcanic areas where drilling is expensive.

Key words: permeability, porous medium, self-potential, streaming potential, water table.

1 INTRODUCTION

In populated volcanic areas, water supply becomes a crucial problem as a result of the increase of consumption associated with an increase of the population densities. In addition, drilling a set of boreholes in a basaltic formation to constrain efficiently the geometry of preferential ground water flow pathways, the depth of the water table and the distribution of the hydraulic transmissivity is a very expensive and difficult task. This explains an emerging interest in developing and using geophysical (non-intrusive) prospecting methods providing complementary hydrogeological information with a minimum of *in situ* calibration data. Among these geophysical methods, a particular attention has been devoted recently to methods sensitive to water saturation and water flow. These include the electrical resistivity tomography (ERT), electromagnetic (EM) methods and the self-potential (SP) methods (e.g. Fournier 1989; Aubert *et al.* 1993; Aubert & Yéné Atangana 1996; Titov *et al.* 2000).

The ERT and EM methods are active methods used to image the DC or the frequency-dependent electrical resistivity distribution inside the ground. In principle, water-saturated rocks should appear more conductive than the same partially saturated rocks located in the vadose zone. However electrical resistivity measurements do not perform well to determine the shape of the ground water level. This is because saturation, hence electrical conductivity, already starts to increase in the vadose zone, as a result of capillary effects and evaporation. So electrical conductivity rarely shows a sharp change across the water table.

The SP method consists of the passive measurements of the electrical potential distribution at the ground surface. This distribution shows usually electrical potential anomalies termed SP anomalies. These anomalies are associated with natural polarization mechanisms occurring at depth. The most important SP anomalies (several hundreds of mV) are redox in nature and associated with ore deposits (e.g. Furness 1992, 1993) and contaminant plumes (Naudet *et al.* 2003). Hydrothermal systems also generate strong SP anomalies associated with the vorticities of the convection pattern (e.g. Revil *et al.* 2004). Some hopes have been also formulated concerning the use of the SP method in hydrogeology. Indeed, in absence of the redox component, the main contribution to the SP signals is usually associated with ground water flow through the electrokinetic (hydroelectric) coupling (e.g. Jouniaux *et al.* 2000; Revil *et al.* 2002; Trique *et al.* 2002, and references therein). The SP method is non-destructive, fast, inexpensive and very simple to implement in the field requiring only a few non-polarizing electrodes and a high internal impedance voltmeter. In addition, electrical noise is usually low in volcanic areas, which implies a good signal-to-noise ratio as discussed below.

Despite the recent development of some inverse algorithms applied to the interpretation of SP anomalies (e.g. Sailhac & Marquis 2001), there is still some debate about the origin of SP signals related to ground water flow and their interpretation in terms of water table elevation. Zablocki (1978) and Jackson & Kauahikaua (1987) assume that SP signals are mainly related to the distance along which water percolates vertically through the vadose zone before reaching the water table. Based on these preliminary works, Aubert *et al.* (1993) developed an interpretation scheme called the self-potential surface (SPS) method in which the SP sources were assumed to be located into the vadose zone. In contrast, Fournier (1989) assumed that the main SP contribution was located along the water table and that the variations of the hydraulic head were directly responsible for the electrical potential anomalies measured at the ground surface.

In this paper, we discuss a model connecting SP signals to the shape of the water table. An optimization algorithm based on the Simplex method is used to invert SP data in terms of water table elevation. This algorithm is applied to a case study corresponding to the site of Marelongue, which is located on the south flank of the Piton de la Fournaise volcano, a large shield volcano on Réunion island in the Indian ocean. This site was chosen for its accessibility and for the number of previous geophysical and hydrogeological investigations made in this area to detect preferential ground water circulations (e.g. Aubert *et al.* 1993; Boubekraoui *et al.* 1998; Boubekraoui & Aubert 1999, and references therein).

2 WATER TABLE FROM SELF-POTENTIAL

2.1 Contribution associated with the water table

We note Ω_i the internal region of the ground in which fluid flow occurs, Ω_e the external region and $\partial\Omega$ the interface between Ω_i and Ω_e: consequently $\partial\Omega$ represents the water table (Fig. 1). Of course, the water table is, strictly speaking, not a sharp interface as a result of the existence of the capillary fringe. We choose deliberately to neglect these effects in the present work.

From thermodynamic arguments, the total electrical density $\mathbf{J}$ in an isotropic porous material is always the sum of a conductive current, described by the Ohm's law, and a net (or driving) source current density $\mathbf{J}_S$. This driving current source is presently associated with the pore fluid pressure field. Therefore, the total current density is given by (e.g. Titov *et al.* 2000; Revil 2002, and references therein)

$$\mathbf{J} = -\sigma(\nabla\varphi - C\nabla p), \tag{1}$$

$$C \equiv -L/\sigma. \tag{2}$$

In eqs (1) and (2), φ and p are the electrical potential (expressed in V) and the fluid pressure (in Pa), respectively, σ is the electrical conductivity of the porous rock (in S m^{-1}), C is the electrokinetic coupling coefficient (expressed in V Pa^{-1}) (see Jouniaux *et al.* 2000, for some laboratory data), L is an electrokinetic coupling term (in A Pa^{-1} m^{-1}) and $\mathbf{J}_S = -L\nabla p = \sigma C\nabla p$ is the electrokinetic current

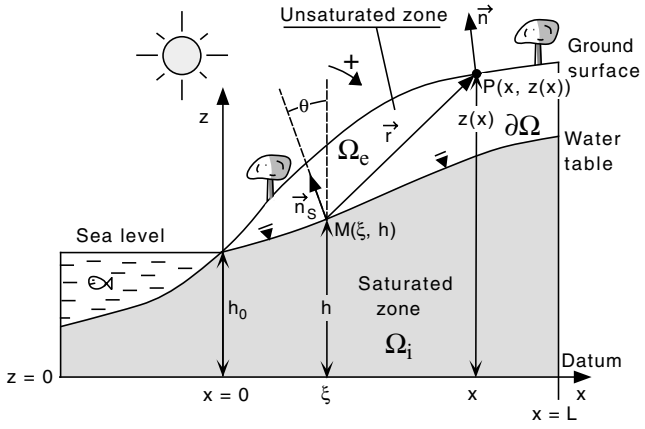

Figure 1. Sketch indicating the position of the water table and the position of the ground surface. In our model, the self-potential (SP) signal measured at point P located at the ground surface (or possibly in a borehole) is the convolution of all the dipolar electrokinetic sources associated with the phreatic surface indicated by the small inverted triangles. The unit vectors $\mathbf{n}$ and $\mathbf{n}_S$ are outward vectors normal to the ground surface and water table, respectively.

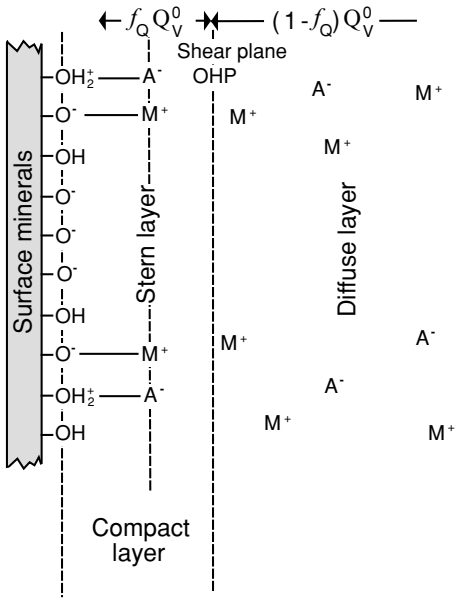

Figure 2. Electrical double layer coating the surface of the grains. The electrical double layer comprises the Stern layer and the Gouy–Chapman diffuse layer, $A-$ and $M+$ correspond to the anions and cations, respectively. The zeta potential represents the potential at the shear plane where the hydrodynamic velocity of the pore fluid is zero. The charge density $\bar{Q}_V^0$ is the fraction of the excess charge contained in the (Gouy–Chapman) diffuse layer per unit pore volume, Q_V^0 is the total excess charge per unit pore volume balancing the deficit of charges of the minerals, which is in turn directly connected to the cation exchange capacity (CEC) of the minerals, and f_Q is the fraction of the countercharge contained in the Stern layer (see Revil & Leroy 2004). The excess of positive versus negative charges in the Gouy–Chapman diffuse layer reflect a global positive (excess) charge in this layer. This positive charge can be drag by the pore water when flowing through the porous material.

source density (in A m^{-2}), which acts as a source term for electromagnetic disturbances in the Maxwell equations. The microscopic origin of the hydroelectrical coupling described by eq. (1) is associated with the drag of the excess of electrical charges contained in the Gouy–Chapman diffuse layer (Fig. 2). In this section, we will ignore potential contributions to SP signals located in the vadose zone (see Section 2.2 below).

Using eq. (1) and the continuity equation $\nabla\cdot\mathbf{J} = 0$ (conservation of charge in the quasi-static limit of the Maxwell equations), we obtain

$$\nabla\cdot(\sigma\mathbf{E}) = \Im, \tag{3}$$

$$\Im = -\nabla\cdot(C\sigma\nabla p) = \nabla L\cdot\nabla p + L\nabla^2 p, \tag{4}$$

where $\mathbf{E} = -\nabla\varphi$ represents the electrical field in the quasi-static limit of the Maxwell equations and $\Im$ (in A m^{-3}) represents the volumetric density of current sources.

In the zone of saturation, we assume that the only body force is the gravitational field. In this situation, the driving force for ground water flow is the hydraulic head h related to the elevation head z and to the pressure head, $\psi \equiv p/\rho_f g$ (ρ_f is the bulk density of the pore water), by $\psi = h - z$ (e.g. Domenico & Schwartz 1997). The electro-osmotic contribution to ground water flow is orders of magnitude smaller than the pressure head contribution in most rocks in absence of external sources of electrical field (Revil 2002). Neglecting safely

this contribution, the fluid flow is governed by the classical diffusion equation (e.g. Domenico & Schwartz 1997, chapter 4),

$$\nabla^2 h - \frac{1}{\eta_H}\frac{\partial h}{\partial t} = \frac{Q}{K}, \tag{5}$$

where Q (in m^3 s^{-1}) is the bulk source term (e.g., infiltration from the vadose zone), $\eta_H = K/S_S$ (in m^2 s^{-1}) is the hydraulic diffusivity, $K = k\rho_f g/\eta_f$ is the hydraulic conductivity (in m s^{-1}), η_f (in Pa s) is the dynamic viscosity of the pore water, k is the permeability, g is the acceleration of the gravity and S_S is the specific storage (in m^{-1}) defined by $S_S = \rho_f g(\beta_p + \phi\beta_f)$ where β_p represents the pore compressibility, ϕ is the porosity and β_f is the compressibility of the pore water (Domenico & Schwartz 1997, chapter 4). Therefore, the volumetric density of current source is simply given by

$$\Im = -\nabla \cdot \mathbf{J}_S, \tag{6}$$

$$\Im = \rho_f g(\nabla L \cdot \nabla h + L\nabla^2 h). \tag{7}$$

The volume density of current source can be also expressed in terms of an equivalent volume distribution of dipole moment, $\Im = -\nabla \cdot \mathbf{P}$ (in A m^{-3}), where $\mathbf{P}$ is an equivalent polarization vector. The continuity equation becomes

$$\nabla \cdot (\sigma \mathbf{E}) = \begin{cases} -\nabla \cdot \mathbf{P}, \mathbf{r} \in \Omega_i, \\ 0, \mathbf{r} \in \Omega_e, \end{cases} \tag{8}$$

where Ω_i is the source region in which fluid flow takes place and bounded at its top by the water table (Ω_e corresponds to the vadose zone, Fig. 1). We assume a piecewise conductivity distribution in a half-space as shown in Fig. 1. With these assumptions, eq. (8) becomes

$$\nabla^2 \varphi(\mathbf{r}) = \begin{cases} \nabla \cdot \mathbf{P}(\mathbf{r})/\sigma_i, \mathbf{r} \in \Omega_i, \\ 0, \mathbf{r} \in \Omega_e, \end{cases} \tag{9}$$

where, in this preliminary investigation, we did not account for any surface of electrical conductivity discontinuity in the region Ω_e external to the source region. The boundary condition at the ground surface is $\mathbf{n} \cdot \nabla\varphi = 0$. The boundary conditions at the piezometric surface $\partial\Omega$ are

$$(\mathbf{J}_e - \mathbf{J}_i) \cdot \mathbf{n}_S = \mathbf{P} \cdot \mathbf{n}_S, \tag{10}$$

$$(\sigma_i \nabla\varphi_i - \sigma_e \nabla\varphi_e) \cdot \mathbf{n}_S = \mathbf{P} \cdot \mathbf{n}_S, \tag{11}$$

where $\mathbf{n}_S$ is the outward normal to the source body (Fig. 1). According to eq. (10), the piezometric surface is characterized by a jump in the normal component of the electrical current density. We can therefore associate a distribution of dipoles to this surface. The Green's function of the Poisson equation is the solution of

$$\nabla^2 G(\mathbf{r}, \mathbf{r}') = \delta^3(\mathbf{r} - \mathbf{r}'), \tag{12}$$

where $\delta^3(\mathbf{r} - \mathbf{r}')$ represents the 3-D Dirac distribution at source point $M(\mathbf{r}')$. The Green's function solution of eq. (12) for a homogeneous half-space (remember that the boundary condition at the ground surface is $\mathbf{n} \cdot \nabla\varphi = 0$, which requires image sources in the atmosphere) is given by

$$G(\mathbf{r}, \mathbf{r}') = -\frac{1}{4\pi}\left(\frac{1}{|\mathbf{r} - \mathbf{r}'|} + \frac{1}{|\mathbf{r} - \mathbf{r}''|}\right), \tag{13}$$

where $\mathbf{r}''$ is the mirror image of the source point $\mathbf{r}'$. If the topography of the ground is relatively small, the previous Green's function reduces to

$$G(\mathbf{r}, \mathbf{r}') = -\frac{1}{2\pi}\frac{1}{|\mathbf{r} - \mathbf{r}'|}. \tag{14}$$

We look for a representation theorem connecting the measured electrical potential at the ground surface to the half-space Green function and electrical potential distribution at depth. To do so, one first notes that everywhere throughout $\Omega_i + \Omega_e$, the electrical potential is given by $\nabla \cdot [\sigma(\mathbf{r})\nabla\varphi] = (\nabla \cdot \mathbf{P})H(z - h)$ where $H(z - h)$ is the Heaviside (step) function with a step at the phreatic surface, $z - h$ represents the depth of the pheatic surface to the ground surface, and where $\sigma(\mathbf{r}) = \sigma_e + H(z - h)(\sigma_i - \sigma_e)$. Using the definition of the unit normal vector to the step surface, $\mathbf{n}\delta(z - h) = \nabla H(z - h)$, one then obtains through standard manipulations (e.g. Furness 1992, 1993; Sobolev 1989)

$$\begin{aligned}\varphi(\mathbf{r}) = {} & \frac{1}{\sigma_e}\int_{\Omega_i} G(\mathbf{r}, \mathbf{r}')\nabla' \cdot \mathbf{P}(\mathbf{r}')\, dV \\ & - \frac{1}{\sigma_e}\int_{\partial\Omega} \mathbf{P}(\mathbf{r}') \cdot \mathbf{n}_S G(\mathbf{r}, \mathbf{r}') dS \\ & - \frac{\sigma_e - \sigma_i}{\sigma_e}\int_{\partial\Omega} \varphi(\mathbf{r}')\mathbf{n}_S \cdot \nabla' G(\mathbf{r}, \mathbf{r}')\, dS \\ & + \int_{z=0} \mathbf{n} \cdot [G(\mathbf{r}, \mathbf{r}')\nabla'\varphi_e(\mathbf{r}') - \varphi_e(\mathbf{r}')G(\mathbf{r}, \mathbf{r}')]\, dS, \end{aligned} \tag{15}$$

$$\begin{aligned}\varphi(\mathbf{r}) = {} & -\frac{1}{\sigma_e}\int_{\Omega_i} \mathbf{P}(\mathbf{r}') \cdot \nabla' G(\mathbf{r}, \mathbf{r}')\, dV \\ & + \left(\frac{\sigma_i - \sigma_e}{\sigma_e}\right)\int_{\partial\Omega} \varphi(\mathbf{r}')\mathbf{n}_S(\mathbf{r}') \cdot \nabla' G(\mathbf{r}, \mathbf{r}')\, dS. \end{aligned} \tag{16}$$

The boundary condition for the electrical potential at the ground surface and the construction of the Green's function ensure that the last term in eq. (15) at the Earth's surface vanishes. After some algebraic manipulations, eq. (16) yields

$$\begin{aligned}\varphi(\mathbf{r}) = {} & -\frac{\sigma_i}{\sigma_e}\int_{\partial\Omega} \Delta\varphi(\mathbf{r}')\mathbf{n}_S(\mathbf{r}') \cdot \nabla' G(\mathbf{r}, \mathbf{r}')\, dS \\ & - \left(\frac{\sigma_e - \sigma_i}{\sigma_e}\right)\int_{\partial\Omega} \varphi_e(\mathbf{r}')\mathbf{n}_S(\mathbf{r}') \cdot \nabla' G(\mathbf{r}, \mathbf{r}')\, dS, \end{aligned} \tag{17}$$

where the potential is defined to an additive constant of integration and where

$$\Delta\varphi(\mathbf{r}') \equiv \varphi_e(\mathbf{r}') - \varphi_i(\mathbf{r}') \tag{18}$$

is a drop in the electric potential through the interface $\partial\Omega$.

If we assume now that the resistivity of the vadose zone is much higher than the resistivity of the aquifer, so $\sigma_e \ll \sigma_i$, then the electrical potential experienced at the observation point $P(\mathbf{r})$ is

$$\varphi(\mathbf{r}) = C'\Theta\int_{\partial\Omega} h(\mathbf{r}')\mathbf{n}_S(\mathbf{r}') \cdot \nabla' G(\mathbf{r}, \mathbf{r}')\, dS, \tag{19}$$

where we have used $-\Delta\varphi(\mathbf{r}') + \varphi_e(\mathbf{r}') = \varphi_i(\mathbf{r}') = C'h(\mathbf{r}')$ and

$$C' \equiv (\partial\varphi/\partial h)_{\mathbf{J}=0} = C\rho_f g, \tag{20}$$

where C' (expressed in mV m^{-1}) measures the sensitivity between the electrical potential φ and the hydraulic head h. It is simply proportional to the electrokinetic coupling coefficient defined by eqs (1) and (2). The assumption that the electrical potential is proportional to the fluid pressure field below the water table requires an explanation. Indeed, this is the case only if these two potentials satisfy the same boundary conditions in the aquifer, which usually they do not. However, we assume here that this is a correct first-order approximation that will need to be further evaluated by numerical modelling. We name the parameter,

$$\Theta \equiv \sigma_i/\sigma_e, \tag{21}$$

the conductivity ratio. For a high conductivity ratio $\Theta \gg 1$ (that we name the HCR-limit below), it is clear from eq. (19) that Θ impacts strongly on the strength of the SP signals recorded at the ground surface. In this situation, high-resolution ERT is a necessary tool to determine the electrical conductivity contrast between the vadose zone and the aquifer and to determine Θ.

We assume now the case where the electrical conductivity is uniform [that we call the uniform conductivity (UC-) limit below]. In the limit $\sigma_e = \sigma_i$, the measured electrical potential at observation point $P(\mathbf{r})$ is given from eq. (17) by

$$\varphi(\mathbf{r}) = -\int_{\partial\Omega} \Delta\varphi(\mathbf{r}')\mathbf{n}_S(\mathbf{r}') \cdot \nabla' G(\mathbf{r}, \mathbf{r}')\, dS, \tag{22}$$

$$\varphi(\mathbf{r}) = (C' - C'_S)\int_{\partial\Omega} h(\mathbf{r}')\mathbf{n}_S(\mathbf{r}') \cdot \nabla' G(\mathbf{r}, \mathbf{r}')\, dS, \tag{23}$$

$$\Delta\varphi(\mathbf{r}) = C'\int_{\partial\Omega} h(\mathbf{r}')\mathbf{n}_S(\mathbf{r}') \cdot \nabla' G(\mathbf{r}, \mathbf{r}')\, dS, \tag{24}$$

where $\Delta\varphi\ (\mathbf{r}') = (C' - C_S')h(\mathbf{r}')$ (eq. 6 in Fournier 1989), C' is the electrokinetic coupling coefficient at saturation (in the aquifer), while C'_S is the electrokinetic coupling coefficient in the vadose zone. Recently, Revil & Cerepi (2004) showed that the streaming potential coupling coefficient is proportional to the water saturation. Consequently, in the case of capillary fringes, we cannot neglect C'_S by comparison with C'.

The UC-limit corresponds to the Fournier's model (Fournier 1989; Birch 1998; Revil *et al.* 2003). Using the 3-D Green's function and assuming that the slope of the ground surface is small, eqs (19) and (22) become

$$\varphi(\mathbf{r}) = C'\Theta\int_{\partial\Omega} h(\mathbf{r}')\mathbf{n}_S(\mathbf{r}') \cdot \nabla' G(\mathbf{r}, \mathbf{r}')\, dS, \tag{25}$$

$$c' = C'\Theta - C'_S \tag{26}$$

for the HCR- and the UC-limits, respectively. We define therefore an apparent coupling coefficient c',

$$c' \equiv C'\left(\frac{2 - \Theta^2}{\Theta}\right). \tag{27}$$

The closed form solution for the electrical potential becomes

$$\varphi(\mathbf{r}) \approx \frac{c'}{2\pi}\int_{\partial\Omega} h(\mathbf{r}')\left(\frac{\mathbf{n}_S(\mathbf{r}') \cdot \mathbf{x}}{x^3}\right) dS, \tag{28}$$

where $\mathbf{x} \equiv \mathbf{r} - \mathbf{r}'$, $x \equiv |\mathbf{r} - \mathbf{r}'|$. In the field, we can not measure an absolute value of the electrical potential and all the data will be referenced to an arbitrary reference, e.g. an electrode located at the sea level where $h = 0$.

As long as the fluctuations of the hydraulic head are larger than the variations of the depth of the water table (small topography), we can take a linear approximation of eq. (28). This yields a first-order linear relationship between the piezometric level and the electrical potential measured at the ground surface,

$$h(x, y) \approx \varphi(P)/c'. \tag{29}$$

This linear approximation will be used later to initiate the optimization algorithm for the complete integral equation.

2.2 Contribution associated with the vadose zone

In a general case, the SP signal recorded at the ground surface will be the sum of a component associated with the downflow of water through the vadose zone plus the component associated with ground water flow in the free aquifer (and eventually a contribution associated with recharge/discharge areas of confined aquifers). Aubert and co-workers (e.g. Aubert *et al.* 1993; Zhang & Aubert 2003, and references therein) have proposed the idea that SP signals found their origin in the vadose zone. They developed a conceptual model in which the vadose zone appears uniformly polarized.

However, in most cases, we expect that the vertical drainage in the vadose zone would not produce strong SP variations at the ground surface except just transiently after a strong rain and in the case of strong infiltration capacity of the topsoil. Indeed, for poorly mineralized waters, there is a strong reduction of the absolute strength of the electrokinetic coupling coefficient with the decrease of the water saturation as shown recently by a set of experiments performed on an unconsolidated sand by Guichet *et al.* (2003) and with some consolidated rocks by Revil & Cerepi (2004). The latest work is based on the model of Revil & Leroy (2004) in which the macroscopic equations were obtained at the macroscopic scale by volume averaging the local (phase-scale) equations.

3 INVERSE METHOD

In this section, we investigate the properties of the integral equation determined in Section 2 and we develop an inversion scheme to reconstruct the shape of the water table. Eq. (28) is written as

$$\varphi(P) = \int_{\partial\Omega} s(M)\psi(P, M)\, dS, \tag{30}$$

$$s(M) \equiv c'h(M), \tag{31}$$

$$\psi(P, M) \equiv \mathbf{n}_S \cdot \mathbf{G}(P, M) = \frac{1}{2\pi}\frac{\mathbf{n}_S \cdot \mathbf{x}}{x^3}, \tag{32}$$

where $\mathbf{G}(P, M)$ and $\psi(P, M)$ are the Green's functions for the SP electrokinetic problem and $s(M)$ is the density of SP sources at point M. Eq. (28) is known as a Fredholm equation of the first kind where $\varphi(P)$ is a linear function of $s(M)$. For all $P \neq M$, $\psi(P, M)$ is a smoothly varying function that makes $\varphi\ (P)$ always smoother than $s(M)$ or $h(M)$, where P is taken at the ground surface and M underlines the position of the water table.

Calculation of $s(M)$ and therefore computation of $h(M)$ if c' is known or guessed, corresponds to the inverse problem. In terms of the inverse problem, as discussed by Blakely (1996), potential field inversion is by nature unstable. In the present case, this means that small errors in $\varphi(P)$ would cause large and unrealistic variations in the geometry of the phreatic surface $h(M)$. In addition, it is well known that the inverse problem associated with the Fredholm equation of the first kind has no unique inverse solution. However non-uniqueness can be reduced, if not removed, if for example the solution is known at some locations (e.g. at least in one borehole), which will be the case in Section 5.

We propose here to recover the depth of the water table by minimizing the following rms cost or objective function E,

$$\mathrm{Min}E^2 \equiv \frac{1}{N}\sum_{i=1}^{N}(\varphi(P_i) - \varphi(P_i)')^2, \tag{33}$$

subject to the constraint $0 \leq h(x) < z(x)$, $\varphi(P_i)$ are the measured electrical potentials and $\varphi(P_i)'$ are the potentials determined from

the 2-D integral equation

$$\varphi(P) = \frac{c'}{2\pi} \int_{\partial\Omega} h \frac{\mathbf{x} \cdot \mathbf{n}_S}{x^2} d\xi. \tag{34}$$

In this equation, ξ represents the curvilinear coordinate along the phreatic surface defined in Fig. 1. We have assumed that variation in direction y can be neglected for the field case investigated below. Eq. (34) is a 2-D version of eq. (28). Eq. (33) represents the quadratic difference between the measured electrical potentials at stations $P_i (1 \leq i \leq N)$ and that determined from the model, where N represents the number of measurements performed at the ground surface. The residual field $e_i = \varphi(P_i) - \varphi(P_i)'$ yields a spatial view of the quality of the model. An overall error evaluation (dimensionless) is provided by the goodness-of-fit parameter,

$$r = \frac{\sum_{i=1}^{N} |\varphi(P_i)|}{\sum_{i=1}^{N} |e_i|}. \tag{35}$$

To find the minimum of E, we have the choice among many types of algorithms. We used here the optimization algorithm SIMP of Caceci & Cacheris (1984). This algorithm is based on the Simplex method and on the least-square criterion. The *a priori* solution needed by the algorithm is determined from the SP data using the first-order linear approximation given by eq. (29) of the integral equation relating the SP to the piezometric head ($h_0 = 0$ if the reference potential is taken at sea level) and an *a priori* value for c'. Synthetic tests show an excellent convergence of the model for different *a priori* models, which implies a well-posed problem and robustness of the method applied to the present problem.

Table 1. Electrokinetic coupling coefficient of basalt samples with NaCl solutions. Measurements were made at 20 ± 2 °C.

	C' (in mV m^{-1})		
σ_f (in S m^{-1})	100–200 μm	200–400 μm	400–630 μm
0.001	−189	−203	−168
0.004	−106	−99	−85.3
0.010	−25.5	−22.6	−20.6
0.050	−2.05	−1.98	−1.95

4 THE COUPLING COEFFICIENT

Before testing the previous method, we determined some possible values for the electrokinetic coupling coefficient. This coupling coefficient is nothing other than a measure of the sensitivity between the electrical potential difference produced in response to a pore fluid pressure gradient, in drained conditions, the rock system being electrically open. Therefore, we performed a set of laboratory experiments to determine the order of magnitude of the streaming potential coupling coefficient C for samples taken from the field site on Réunion island, investigated below in Section 5.

The samples were poorly altered basalts. The samples were crushed, washed to remove the organic matter and sieved. Three ranges of grain size were kept for the measurements, 100–200, 200–400 and 400–600 μm. The samples were saturated with NaCl electrolyte at different ionic strengths. Measurements were performed with the ZetaCad^{TM} apparatus (Fig. 3a). The results are shown in Fig. 3 and in Table 1. The results indicate that the coupling coefficient depends strongly on the electrical conductivity of the pore water saturating its connected porosity as expected from the theory

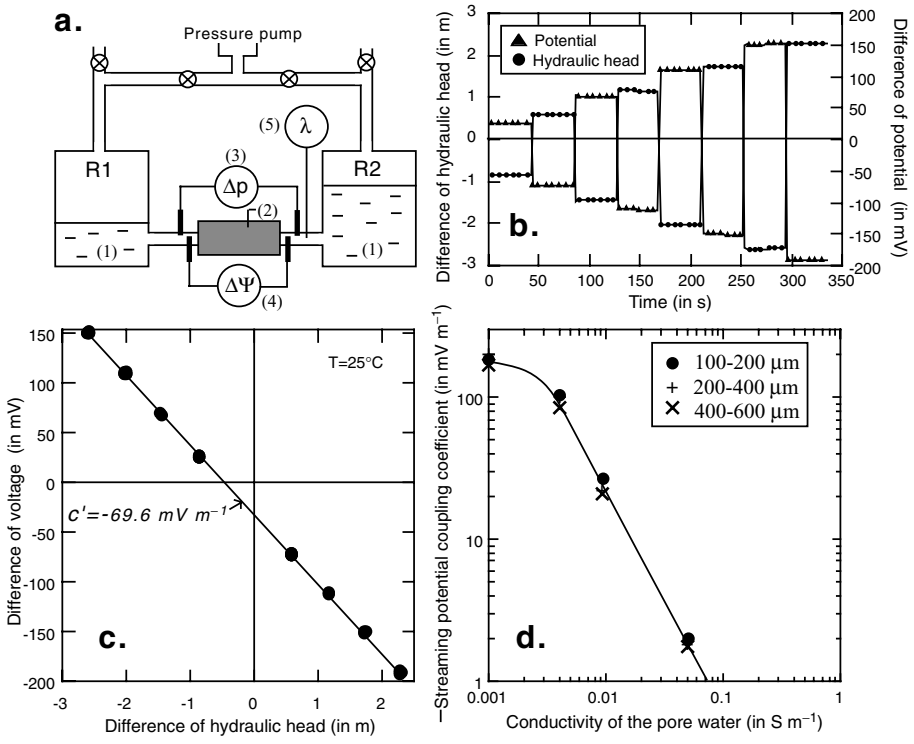

Figure 3. Laboratory measurements of C'. (a) Sketch of the experimental setup (ZetaCad^{TM}). (1) Pore fluid reservoirs R1 and R2; (2) sample tube; (3) pressure sensors, (4) voltage non-polarizable electrodes connected to an impedance meter, (5) measurements of the electrical conductivity of the electrolyte. The pressure is controlled with nitrogen gas, which has no effect on the pH and salinity of the electrolyte. The equipment is controlled by a desktop computer. (b, c) Typical run for which the electrical potential measured at the end faces of the core is reported as a function of the hydraulic head. Error bars are less than the size of the circles. (d) The electrokinetic coupling coefficient C' is plotted versus the electrical conductivity of the water.

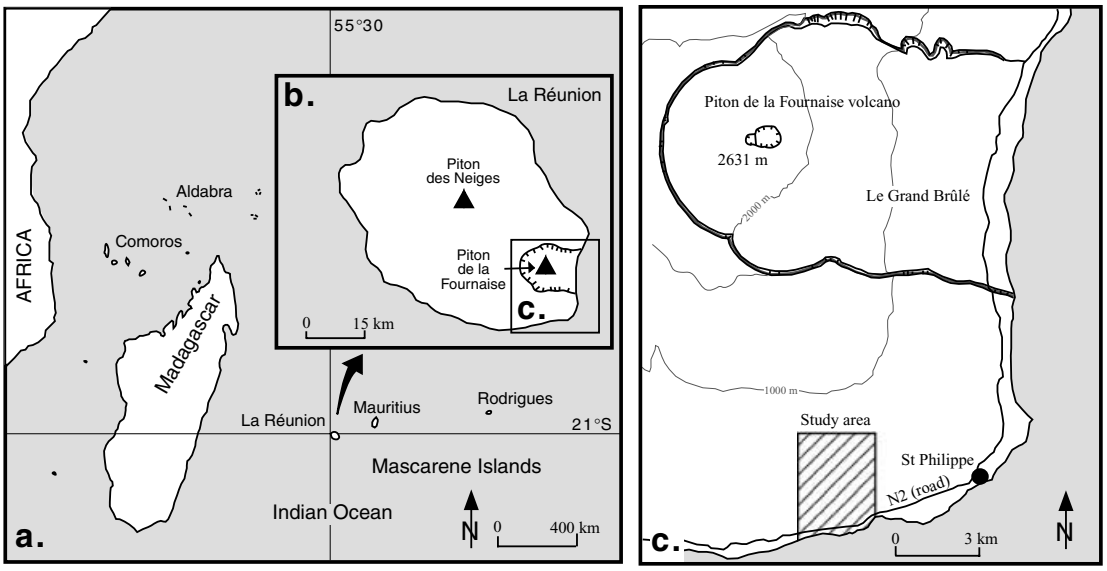

Figure 4. Location of the Réunion island in the Mascarene archipelago (Indian ocean). (b) Location of the Piton de la Fournaise volcano. (c) Location of the study area (Mare Longue natural reserve), on the south flank of the Piton de la Fournaise volcano.

(Revil 2002; Revil *et al.* 2003). It varies typically between −80 to −1 mV m^{-1} depending on the salinity of the pore water.

In the next field case, the electrical conductivity of the ground water on the flanks of the Piton de la Fournaise volcano was found in the range (3–12) × 10^{-3} S m^{-1} with an average value of 8 × 10^{-3} S m^{-1} (Hoareau 2001). Therefore, according to Fig. 3, C' is in the range −15 to −68 mV m^{-1} with an average value equal to −24 mV m^{-1}. Taking eq. (27) with $\Theta = 1$ and $C'_S = -17$ mV m^{-1} (70 per cent of water saturation just above the water table) yields a value of c' equal to −7 mV m^{-1}, that we will use as an *a priori* value in Section 5.

5 CASE STUDY

The Réunion island is the largest volcanic island of the Mascarene archipelago. It is located 800 km east of Madagascar (Fig. 4). The site is located on the natural reserve of Mare Longue located on the southern flank of the active Piton de la Fournaise volcano (the position of study area is 21°20′S latitude and 55°45′N longitude, see Figs 4 and 5). The mean annual rainfall at Mare Longue is ∼4 m per year. The test field stretches from sea level to ∼550 m above seael and corresponds to a primary forest corridor flanked by several sugarcane fields. This primary forest develops on a pahoehoe-type (relatively unaltered) basaltic lava flow whose age is ∼400–600 yr (Bachèlery 1999). The upper volcanic section is built by a pile of long and narrow basaltic lava flows as shown below on the electrical resistivity sections. These lava flows are relatively permeable (Coudray *et al.* 1990).

The SP map (see Figs 5 to 7) is performed with two non-polarizable Petiau Pb/$PbCl_2$ electrodes, comprising a rod of lead immersed in kaolinite saturated by KCl/$PbCl_2$ electrolyte. We used a high impedance millivoltmeter (∼10^8 Ω internal impedance) to carry out the measurements in the field. Before and after each series of measurements, the electrodes were put face to face and then side by side in the same hole to check if the difference in potential was stable and <2 mV (otherwise the static difference between the electrodes was removed from the measurements). The measurements were made using one of the two electrodes as a fixed reference

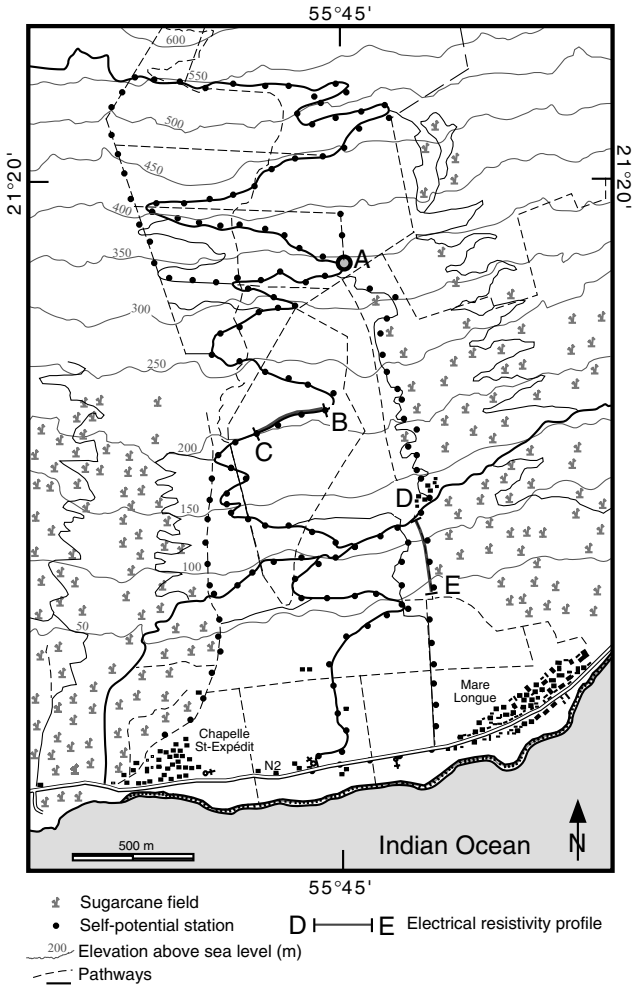

Figure 5. Location of the study area including the position of the self-potential (SP) stations (A is the base station for the whole map) and the position of the two electrical resistivity profiles (BC and DE).

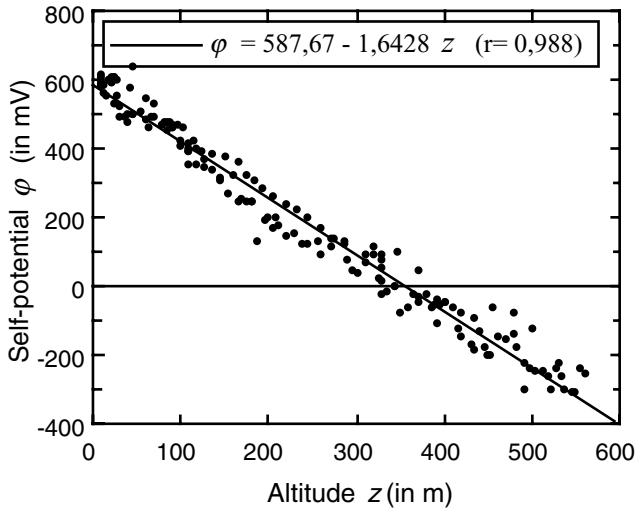

Figure 6. Self-potential (SP; in mV) versus altitude (in m) for the covered area. The linear trend is used to determine the electrical potential difference between the base station A of Fig. 2 and sea level (this electrical potential is equal to ∼588 mV).

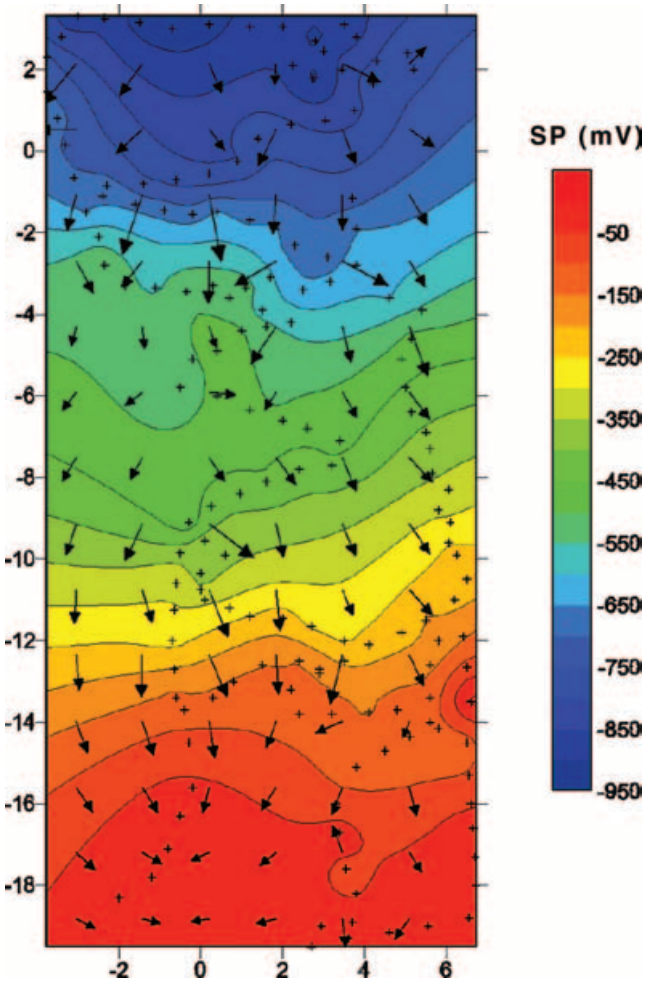

Figure 7. Self-potential (SP) map (in mV) for the covered area. The reference is taken at sea level. Note the existence of preferential fluid flow pathways indicated by valley-like depressions in the SP equipotentials. The crosses represent the position of the SP stations. The arrows represent the opposite of the SP gradient.

station. The second electrode was used to measure the electrical potential at the ground surface along the profile. At each measurement station, a small hole (a few centimetres deep) was dug when this was possible. Otherwise the measurements were made directly on the surface of the basalt. Contacts with the roots of plants were avoided because they can be the source of spurious bioelectric potentials amounting to tens of millivolts in some circumstances. Repeated measurements at each station showed that the standard deviation was sometimes ∼10–15 mV but usually ∼5 mV.

In the present case study, the moisture in the soil was always high enough to make the impedance of the contact between the measuring electrode and the soil or the basalt surface low enough to obtain good measurements. A long cable (700 m) was used to connect the two electrodes. Except for the two profiles shown Figs 8 and 9 (electrode spacing 5 m), the distance between two successive measurements was 100 m. The advantage of this procedure was to avoid cumulative errors by changing the reference too often along the same profile. Every 700 m, a new reference station was settled. All the SP data were referenced to a unique remote base station (point A on Fig. 5) or to sea level; the methodology was similar to that used by Finizola *et al.* (2002).

The present survey comprises 164 measurements. The quality of the measurements can be checked using the fact that the sum of the potential drops should go to zero along a closed loop outside the source region (Kirchoff's law),

$$\oint_C \mathbf{E}\, dl = 0, \tag{36}$$

where C is a closed contour at the ground surface. This was nearly the case here for the five loops used in the present study. When present, the small residual voltage differences (< few tens of mV) were redistributed over the base stations of the loops to close the loops. This corresponds approximately to a residual error of 5 mV per base station (similar to the standard deviation reported above at the measurement station). Then the electrical potential at each station was corrected for these closure errors. This type of procedure should be applied especially in the case of surveys covering large areas, otherwise closure errors can be especially acute. There are many examples of published SP maps showing significant closure errors (several hundred millivolts) between unclosed profiles and resulting from inappropriate use of the leap-frog method.

In addition to the SP survey, we carried out two DC-electrical resistivity tomographies associated with additional high-resolution SP measurements along these profiles (Figs 8 and 9). We used the ABEM Terrameter (SAS-4000, ABEM-France, Rennes), the Wenner-α protocol and a set of 64 standard stainless electrodes. The data were inverted with RES2DINV (Loke & Barker 1996). The electrode spacing in the field was 5 m along the curvilinear coordinate for the two straight profiles. The presence of an aquifer was characterized by low values of the electrical resistivity. Profile DE indicates the depth of the aquifer (characterized by a well-marked boundary for the electrical resistivity around 500 ± 100 Ωm) is ∼50 ± 10 m below the ground surface at an altitude of 100 m (the electrical resistivity of the ground water is discussed below; Fig. 8). This electrical resistivity range for the aquifer is also in agreement with audiomagnetotelluric (AMT) investigations performed by Boubekraoui *et al.* (1998) who found a conductive layer (200–500 Ωm) overlaid by a resistive body with a resistivity in the range 1.5–3.0 kΩm. In the case of profile BC, we only know that the water table is at least at a depth of 50 m below the ground surface. Note the piles of long and narrow basaltic lava flow tubes, which are very well observed on the ERT (Figs 8 and 9).

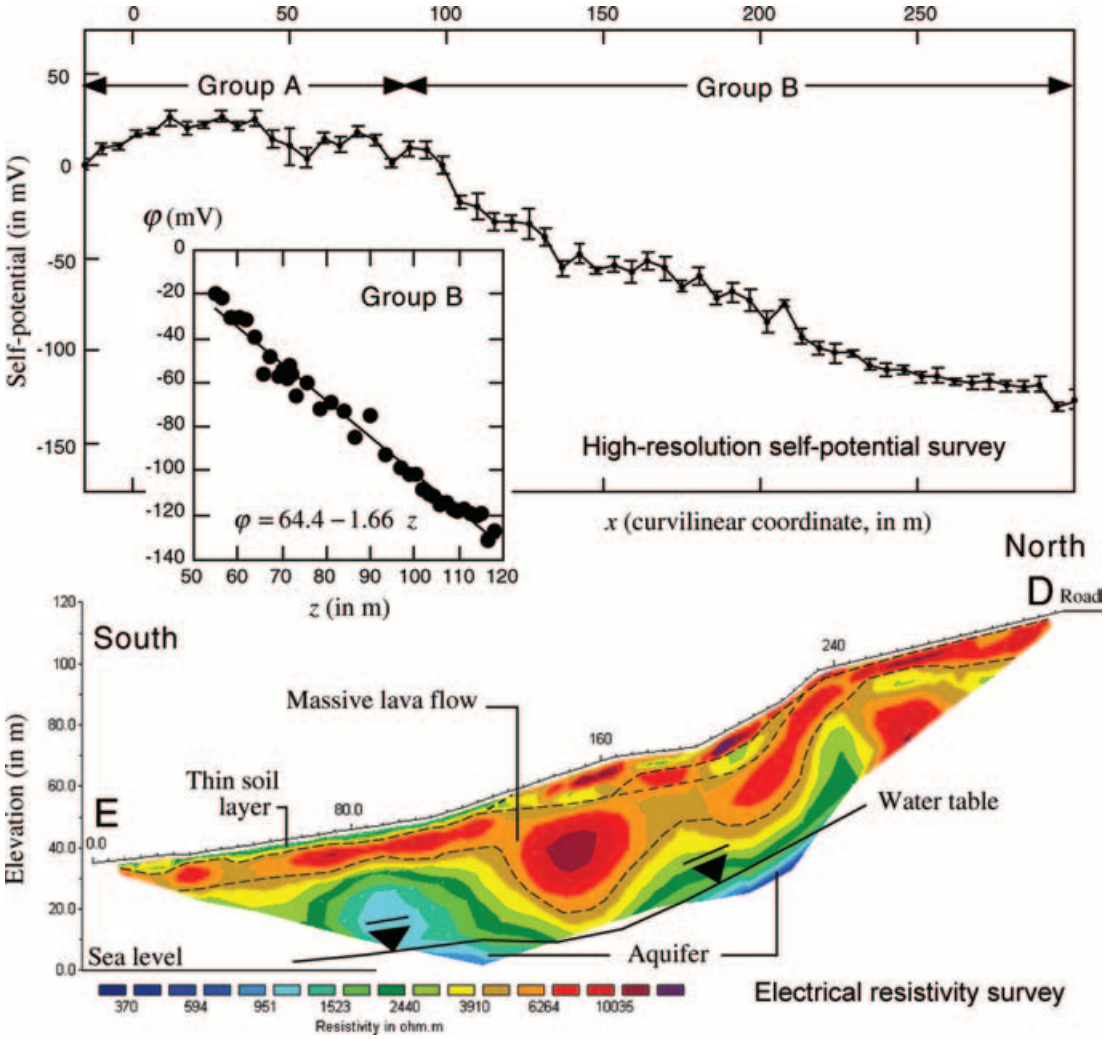

Figure 8. Electrical resistivity and high-resolution self-potential (SP) survey (profile DE). Note that the dependence of the SP signal with the altitude along this profile (-1.66 mV m^{-1}) is nearly the same coefficient for the entire area (see Fig. 3). Groups A and B correspond to different SP/depth relationships. The error bars reported for the SP measurements represent the standard deviations from a set of five measurements at each station and made on a square of 1 m^2.

Application of the Simplex algorithm to the SP data is shown Fig. 10. We have selected an *a priori* value for c' equal to -7 mV m^{-1} (see Section 4). The best estimated value (leading to the smallest residual) is $c' = -5.1$ mV m^{-1}. This value is very close to the optimized value of -4.7 mV m^{-1} determined on the slope of the Kilauea volcano in Hawaii (another shield volcano) from the original data of Jackson & Kauahikaua (1987).

The optimized water table (no free parameters) is in agreement with the position of the water table determined from the ERT shown in Fig. 8 (profile BC). It is especially in agreement with the position of the water table determined from EM surveys (AMT and very low frequency, VLF, methods) performed in the Baril area in the vicinity of the Marelongue area (see Boubekraoui *et al.* 1998 and Boubekraoui & Aubert 1999, especially their figs 9 to 12 where the altitudes should be divided by a factor 2 as a result of a mistake made by the authors). The slope of the water table in the vicinity of the coast is very small (<1 per cent) in agreement with numerical modelling calculations made by Violette *et al.* (1997) for the Piton de la Fournaise volcano. At an altitude of 400 m, it is also in agreement with the piezometric level obtained in a borehole located a few kilometres away, in the Baril area further west from the prospected area.

6 CONCLUDING STATEMENTS

In volcanic areas, the SP method is an economical and fast reconnaissance tool to determine the shape and depth of the water table. This method has been clearly underused as a result of (i) problems with reproducibility associated with the use of poorly designed electrodes (improved field techniques and a new generation of non-polarizable electrodes have virtually eliminated these problems) and (ii) the lack of a model linking the shape of the phreatic surface to the recorded SP anomalies. The present field survey, performed on the flanks of a shield volcano, shows a standard deviation of 5 mV, which is extremely small when compared to the overall amplitude of the signal (~900 mV). This implies a very good signal-to-noise ratio for the collected data set. In addition, the use of the multiple closed-loops method during the acquisition allows checking of the quality of the data and can be used to reduce the propagation and amplification of errors when using the leap-frog technique for the SP measurements.

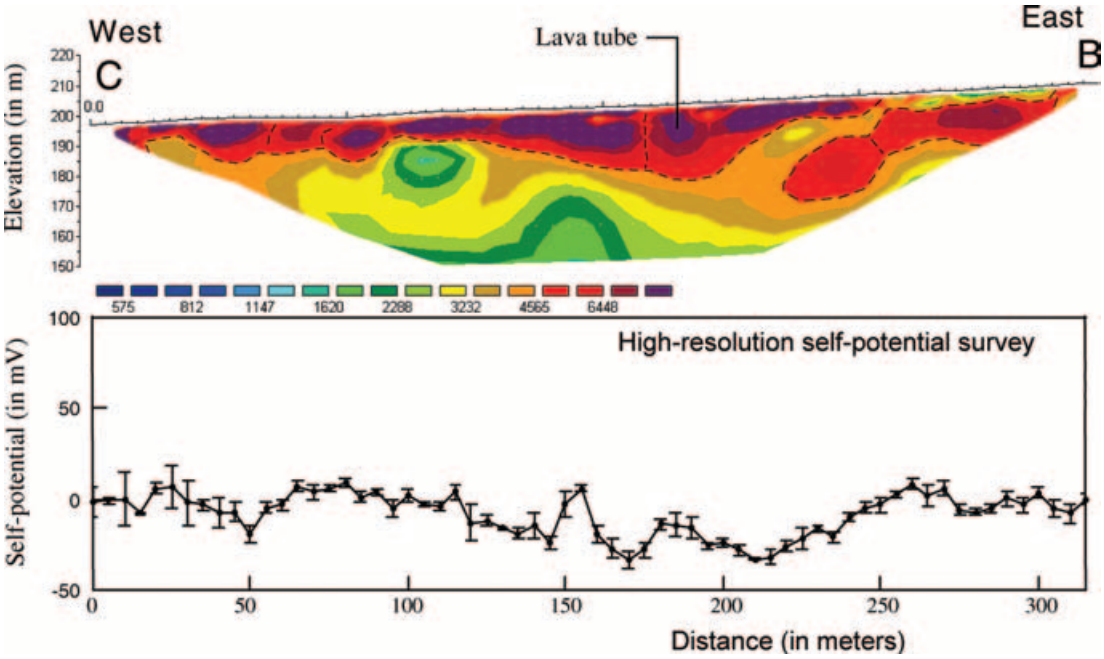

Figure 9. Electrical resistivity and high-resolution self-potential (SP) survey (profile CB) along a profile perpendicular to the slope along an equipotential.

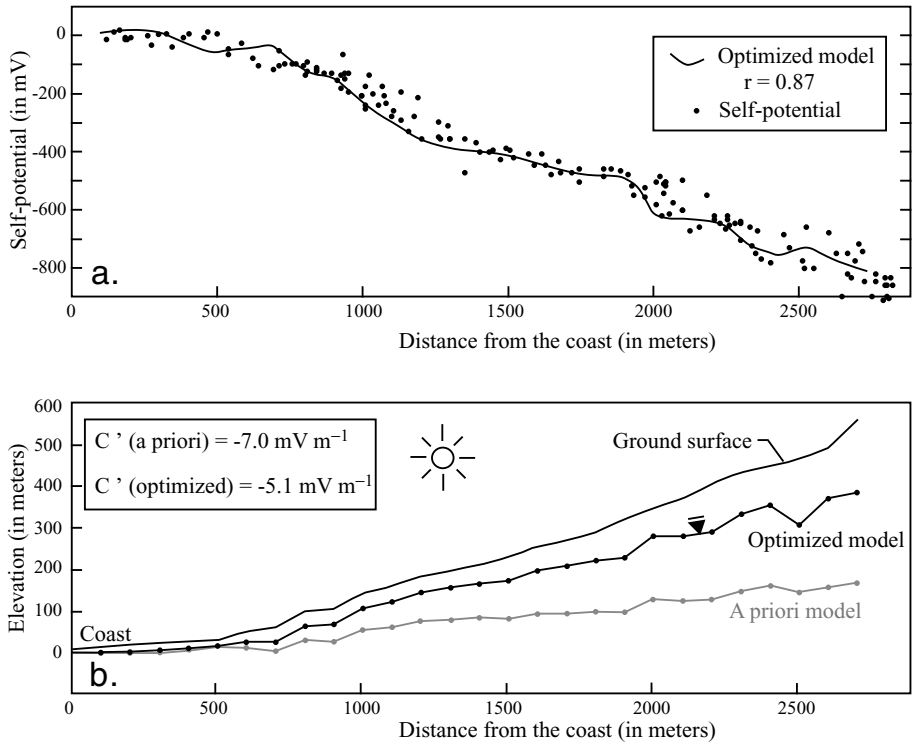

Figure 10. Inversion of the self-potential (SP) data in terms of water table elevation (92 000 iterations). (a) SP data and optimized fit. (b) Position of the water table and ground elevation. Note that at an altitude of 100 m, the water table is roughly at a depth of 40 m, which is consistent with the results displayed on Fig. 8.

In this paper, we have shown that each element of the water table can be seen as a small dipole radiating an electrical field with strength proportional to its elevation. It seems that the water table contribution represents the dominant mechanism producing SP signals on the flanks of volcanic areas. Inversion algorithms developed for potential field problems can be used to reconstruct the shape of the water table from SP data. The next steps will be to extend our inversion algorithm in 3-D and to include the electrical resistivity distribution in the inversion of the SP sources.

ACKNOWLEDGMENTS

We thank E. Nicolini and E. Delcher for their indications relative to the site of Mare Longue and D. Hermitte for his help in the field. We thank A. Finizola, M. Aubert and V. Lapenna for fruitful discussions about geoelectric investigations in volcanic areas. This work was supported by the French National Programs PNSE, ACI Jeune granted to AR and ACI 'Eau et Environnement' granted to AR and D. Gibert. We thank B. Dupré and B. Hamelin for their support. The PhD grant of Véronique Naudet is supported by ADEME (P. Bégassat) in France. We also thank Nicolas Florsch and Konstantin Titov for their help and the two referees for their constructive comments.

REFERENCES

Aubert, M. & Yéné Atangana, Q., 1996. Self-potential method in hydrogeological exploration of volcanic areas, *Ground Water,* **34,** 1010–1016.

Aubert, M., Antraygues, P. & Soler, E., 1993. Interprétation des mesures de polarisation spontanée (PS) en hydrogéologie des terrains volcaniques. Hypothèses sur l'existence d'écoulements préférentiels sur le flanc Sud du Piton de la Fournaise (Ile de la Réunion), *Bull. Soc. Géol. France,* **164,** 17–25 (in French).

Bachèlery, P., 1999. Le fonctionnement des volcans boucliers. Example des volcans de la Réunion et de la Grande Comore, *Thèse d'Habilitation à Diriger des Recherches,* Université de Saint Denis de la Réunion, France (in French).

Birch, F.S., 1998. Imaging the water table by filtering self-potential profiles, *Ground Water,* **36,** 779–782.

Blakely, R.J., 1996. *Potential theory in gravity and magnetic appplications,* Cambridge University Press, Cambridge, p. 441.

Boubekraoui, S. & Aubert, M., 1999. Self-potential method applied to the geological and hydrogeological investigation of shallow structures at Grand-Brûlé (Réunion Island, Indian Ocean), *Hydrogéologie,* **1,** 43–51 (in French).

Boubekraoui, S., Courteaud, M., Aubert, M., Albouy, Y. & Coudray, J., 1998. New insights into the hydrogeology of a basaltic shield volcano from a comparison between self-potential and electromagnetic data: Piton de la Fournaise, Indian Ocean, *J. appl. Geophys.,* **40,** 165–177.

Caceci, M.S. & Cacheris, W.P., 1984. Fitting curves to data, the Simplex algorithm is the answer, *Byte,* **9,** 340–362.

Coudray, J., Mairine, P., Nicolini, E. & Clerc, J.M., 1990. Approche hydrogéologique, in *Le Volcanisme de l'île de la Réunion, Monographie,* Vol. 379, pp. 307–355, ed. Lénat, J.F., Centre de Recherche Volcanologique de Clermont-Ferrand, France (in French).

Domenico, P.A. & Schwartz, F.W., 1997. *Physical and Chemical Hydrogeology,* 2nd edn, John Wiley and Sons, New York.

Finizola, A., Sortino, S., Lénat, J.-F. & Valenza, M., 2002. Fluid circulation at Stromboli volcano (Aeolian Islands, Italy) from self-potential and CO_2surveys, *J. Volc. Geotherm. Res.,* **116,** 1–18.

Fournier, C., 1989. Spontaneous potentials and resistivity surveys applied to hydrogeology in a volcanic area: case history of the Chaîne des Puys (Puy-de-Dôme, France), *Geophys. Prospect.,* **37,** 647–668.

Furness, P., 1992. Modelling spontaneous mineralization potentials with a new integral equation, *J. appl. Geophys.,* **29,** 143–155.

Furness, P., 1993. A reconciliation of mathematical models for spontaneous mineralization potentials, *Geophys. Prospect.,* **41,** 779–790.

Guichet, X., Jouniaux, L. & Pozzi, J.-P., 2003. Streaming potential of a sand column in partial saturation conditions, *J. geophys. Res.,* **108,** 10.1029/2001JB001517.

Hoareau, J.L., 2001. Etude de la minéralisation des eaux naturelles au contact de la série magmatique différenciée de la Réunion. Approches expérimentale et numérique, *PhD thesis,* Université de la Réunion, France, p. 218 (in French).

Jackson, D.B. & Kauahikaua, J., 1987. Regional self-potential anomalies at Kilauea Volcano, *USGS Professional Paper,* **1350,** 947–959.

Jouniaux, L., Bernard, M.-L., Zamora, M. & Pozzi, J.-P., 2000. Streaming potential in volcanic rocks from Mount Pelée, *J. geophys. Res.,* **105,** 8391–8401.

Loke, M.H. & Barker, R.D., 1996. Rapid least-squares inversion of apparent resistivity pseudosections by a quasi-Newton method, *Geophys. Prospect.,* **44,** 131–152.

Naudet, V., Revil, A., Bottero, J.-Y., & Bégassat, P., 2003. Relationship between self-potential (SP) signals and redox conditions in contaminated groundwater, *Geophys. Res. Lett.,* **30**(21), 2091, doi: 10.1029/2003GL018096.

Revil, A., 2002. The hydroelectric problem of porous rocks: thermodynamic approach and introduction of a percolation threshold, *Geophys. J. Int.,* **151,** 944–949.

Revil, A. & Cerepi, A., 2004. Streaming potentials in two-phase flow condition, *Geophys. Res. Lett.,* **31(11),** L11605, doi: 10.1029/2004GL020140.

Revil, A. & Leroy, P., 2004. Governing equations for ionic transport in porous shales, *J. geophys. Res.,* **109,** B03208, doi: 10.1029/2003JB002755.

Revil, A., Hermitte, D., Voltz, M., Moussa, R., Lacas, J.-G., Bourrié, G. & Trolard, F., 2002. Self-potential signals associated with variations of the hydraulic head during an infiltration experiment, *Geophys. Res. Lett.,* **29**(7), 1106, doi: 10.1029/2001GL014294.

Revil, A., Saracco, G. & Labazuy, P., 2003. The volcano-electric effect, *J. geophys. Res.,* **108**(B5), 2251, doi: 10.1029/2002JB001835.

Revil, A., Finizola, A., Sortino, F. & Ripepe, M., 2004. Geophysical investigations at Stromboli volcano, Italy. Implications for ground water flow, *Geophys. J. Int.,* **157,** 426–440.

Sailhac, P. & Marquis, G., 2001. Analytic potentials for the forward and inverse modeling of SP anomalies caused by subsurface fluid flow, *Geophys. Res. Lett.,* **28,** 1851–1854.

Sobolev, S.L., 1989. *Partial Differential Equations of Mathematical Physics,* Dover, New York, p. 427.

Titov, K., Loukhmanov, V. & Potapov, A., 2000. Monitoring of water seepage from a reservoir using resistivity and self-polarization methods: case history of the Petergoph fountain water supply system, *First Break,* **18,** 431–435.

Trique, M., Perrier, F., Froidefond, T., Avouac, J.P. & Hautot, S., 2002. Fluid flow near reservoir lakes inferred from the spatial and temporal analysis of the electric potential, *J. geophys. Res.,* **107,** 10.1029/2001JB000482.

Violette, S., Ledoux, E., Goblet, P. & Carbonnel, J.-P., 1997. Hydrologic and thermal modeling of an active volcano: the Piton de la Fournaise, Réunion, *J. Hydrology,* **191,** 37–63.

Zablocki, C.J., 1978. Streaming potentials resulting from the descent of meteoric water. A possible source mechanism for Kilauean self-potential anomalies, *Geotherm. Res. Council, Trans.,* **2**(2), 747–748.

Zhang, G.-B. & Aubert, M., 2003. Quantitative interpretation of self-potential anomalies in hydrogeological exploration of volcanic areas: a new approach, *Near Surface Geophysics,* **1,** 69–75.